Mantle wedge exhumation beneath the Dora-Maira (U)HP dome unravelled by local earthquake tomography (Western Alps)

Stefano Solarino[1], Marco G. Malusà[2], Elena Eva[1], Stéphane Guillot[3], Anne Paul[3], Stéphane Schwartz[3], Liang Zhao[4], Coralie Aubert[3], Thierry Dumont[3], Silvia Pondrelli[5], Simone Salimbeni[5], Qingchen Wang[4], Xiaobing Xu[4], Tianyu Zheng[4], Rixiang Zhu[4]

[1] *Istituto Nazionale di Geofisica e Vulcanologia, CNT, Genova, Italy*

[2] *Department of Earth and Environmental Sciences, University of Milano-Bicocca, Milano, Italy*

[3] *Université Grenoble Alpes, CNRS, ISTerre, Grenoble, France*

[4] *Institute of Geology and Geophysics, Chinese Academy of Sciences, Beijing, China*

[5] *Istituto Nazionale di Geofisica e Vulcanologia, Bologna, Italy*

Authors for correspondence : S. Solarino and M.G. Malusà (stefano.solarino@ingv.it; marco.malusa@unimib.it)

Abstract

The behaviour of the mantle wedge of continental subduction zones during exhumation of ultra-high pressure (UHP) rocks is still poorly understood. Here, we shed light on this issue by a detailed analysis of the velocity structure of the mantle wedge beneath the Dora-Maira (U)HP dome in the Western Alps, based on local earthquake tomography independently validated by receiver function analysis. Our results point to a composite structure of the mantle wedge above the subducted European lithosphere. The Dora-Maira (U)HP dome lays directly above partly serpentinized peridotites (Vp ~7.5 km/s; Vp/Vs = 1.70-1.72), documented from ~10 km depth down to the top of the eclogitized lower crust of the European plate. To the east, these serpentinized peridotites are juxtaposed against dry mantle peridotites of the Adriatic upper plate along an active fault rooted in the lithospheric mantle. We propose that peridotite serpentinization was due to fluids released from the subducting Alpine slab to the Adriatic mantle wedge. Seismic velocities point to a minor amount of eclogitic metasediments above the European slab, which suggests that the subduction wedge was largely exhumed during late Eocene transtension along the Western Alps subduction zone. Meanwhile, part of the Adriatic mantle wedge was also exhumed at shallow

crustal levels, to be finally indented under the Alpine metamorphic units in the early Oligocene. Our results suggest that mantle-wedge exhumation may represent an important feature of the deep structure of exhumed continental subduction zones. The deep orogenic levels here imaged by seismic tomography may be exposed today in older continental subduction zones, where mantle wedge serpentinites are commonly associated with continental (U)HP metamorphic rocks.

Keywords: continental subduction; ultra-high-pressure metamorphism; mantle wedge exhumation; peridotite serpentinization; local earthquake tomography; Western Alps

Highlights:

- First geophysical evidence of mantle wedge exhumation during continental subduction
- High-resolution image of the seismic velocity structure of the Alpine mantle wedge
- Mantle wedge exhumation is coeval to continental UHP rock exhumation

1. Introduction

Exhumed ultra-high pressure (UHP) units bear compelling evidence of the interaction between subducting plates and the overlying mantle wedge (Carswell and Compagnoni, 2003; Hacker et al., 2006; Ferrando et al., 2009; Scambelluri et al., 2010; Deschamps et al., 2013). However, the role played by the mantle wedge during UHP rock exhumation is still poorly understood. Some numerical models point to a negligible mantle involvement during exhumation (Yamato et al., 2008; Butler et al., 2013), whereas other models suggest that the mantle may be strongly involved and may possibly follow the exumation path of buoyant UHP rocks towards Earth's surface (Schwartz et al., 2001; Petersen and Buck, 2015). A precise observational characterization of the behaviour of the mantle wedge in (U)HP orogenic belts such as the European Alps, where the slab structure is still largely preserved (Zhao et al., 2016a), may thus provide important pinpoints for a better understanding of the mechanisms leading to the exhumation of UHP continental and mantle-

wedge rocks more generally (Agard et al. 2009; Guillot et al., 2009; Liou et al., 2009; Little et al., 2011; Malusà et al., 2011; Warren, 2013).

Here, we shed light on this issue by a detailed analysis of the seismic velocity structure of the mantle wedge beneath the Dora-Maira (U)HP dome in the Western Alps, where coesite, attesting deep continental subduction (e.g., Gilotti, 2013), was first described three decades ago (Chopin, 1984). We exploit a comprehensive seismic dataset, also including anomalously deep earthquakes (Eva et al., 2015), to derive a local earthquake tomography model of the analyzed mantle region, which is then compared with the results provided by receiver function analysis along the CIFALPS transect (China-Italy-France Alps seismic survey; Zhao et al., 2015). Our results suggest that part of the mantle wedge that was metasomatized above the Alpine subduction zone, was subsequently exhumed at shallow depth beneath continental (U)HP rocks now exposed at the surface. These findings suggest that mantle wedge exhumation can be a prominent feature of the deep structure of many orogenic belts, which should be integrated in future theoretical models of continental subduction and UHP rock exhumation. Moreover, our results provide new interpretive keys to understand the field relationships between mantle-wedge rocks and continental UHP rocks in older orogenic belts, where deep crustal levels, here illuminated by geophysical investigations, are possibly exposed by protracted erosional unroofing.

2. Tectonic setting

The Western Alps are the result of oblique subduction of the Alpine Tethys under the Adriatic microplate since the Late Cretaceous, followed by continental collision between the Adriatic and European paleomargins during the Cenozoic (Coward and Dietrich, 1989; Lardeaux et al., 2006; Handy et al. 2010; Malusà et al., 2015). The orogenic wedge exposed along the CIFALPS transect (X-X’ in Fig. 1), in the southern Western Alps, mainly consists of rocks derived from the Piedmont ocean-continent transition and from the adjoining European paleomargin (Lemoine et al., 1986; Dumont et al., 2012). The external zone, exposed to the west of the Frontal Pennine Fault (FPF in

Fig. 1), includes the Pelvoux and Argentera basements and their deformed Meso-Cenozoic sedimentary cover sequences (Ford et al., 2006), which record a transition from thin-skinned to thick-skinned compressional tectonics during the Neogene (Schwartz et al., 2017). East of the Frontal Pennine Fault, in the Alpine metamorphic wedge, the Briançonnais nappe stack (Br in Fig. 1) mainly consists of Upper Paleozoic to Mesozoic metasediments and underlying pre-Alpine basement rocks that underwent subduction starting from the Paleocene, and were later exhumed in the Eocene - early Oligocene (Malusà et al., 2002, 2005; Ganne et al., 2007; Lanari et al., 2014). The Briançonnais nappe stack forms the core of the present-day Alpine fan-shaped structure (Michard et al., 2004) that was overprinted by a dense network of extensional faults during the Neogene (Sue et al., 2007; Malusà et al., 2009). The eastern part of the fan is formed by oceanic metasediments of the Schistes lustrés complex (SL in Fig. 1; Lemoine et al., 1986; Lagabrielle and Cannat, 1990), including boudinaged decametre-to-kilometre-sized ophiolitic bodies that were deformed and metamorphosed during Alpine subduction under blueschist to transitional blueschist–eclogite facies conditions (Agard et al., 2002; Tricart and Schwartz, 2006; Schwartz et al., 2009). A ductile normal fault (Ballèvre et al., 1990) separates the Schistes lustrés complex from the Viso metaophiolites (Vi in Fig. 1; Lombardo et al., 1978; Angiboust et al., 2012), representing major imbricated remnants of the Tethyan oceanic lithosphere that were deformed and metamorphosed under eclogite facies conditions during the Eocene (Duchêne et al., 1997; Schwartz et al., 2000; Rubatto and Hermann, 2003). Another ductile normal fault (Blake and Jayko, 1990) separates the Viso eclogites from the underlying stack of deeply subducted continental basement slices referred to as the Dora-Maira (U)HP dome (DM in Fig. 1; Henry et al., 1993; Michard et al., 1993). This dome includes the coesite-bearing Brossasco-Isasca eclogitic unit (black star in Fig. 1; Chopin et al., 1991; Compagnoni and Rolfo, 2003), which is sandwiched between quartz-bearing eclogite facies rocks, above, and blueschist facies metasediments, below (Avigad et al., 2003). Along the boundary with the Po Plain, the CIFALPS transect crosses the southern tip of the Lanzo massif (La in Fig. 1; Boudier, 1978; Piccardo et al., 2007), an eclogitized mantle slice separated from the Dora-

Maira dome by a vertical active fault system rooted in the upper mantle (Malusà et al., 2017), at the southward prolongation of the Insubric Fault. The Lanzo massif consists of slightly serpentinized spinel plagioclase peridotites surrounded by a 3–5 km thick envelope of foliated serpentinites (Müntener et al., 2004; Debret et al., 2013), and records a high-pressure metamorphic peak of early Eocene age (Rubatto et al., 2008). Beneath the Po Plain, the complex transition zone between the Adriatic upper plate and the Apennines, also involving rotated fragments of the Alpine orogenic wedge (Maffione et al., 2008; Eva et al. 2015), is mainly covered by thick Cenozoic to Quaternary sedimentary successions.

3. Methods

3.1. Building the database

The local earthquake tomography presented in this work is largely based on the dataset collected during the CIFALPS experiment (Zhao et al., 2016b), which was integrated by data recorded in the same time interval by permanent seismic networks operating in Italy and France, and complemented with select older events. The temporary network of the CIFALPS experiment (blue marks in Figure 1B) includes 46 broadband seismic stations deployed along a linear WSW-ESE transect from the European foreland to the western Po Plain, and 9 additional stations installed to the north and to the south of the main profile. Stations operated from July 2012 to September 2013, and were specifically deployed for a direct comparison between receiver function and local earthquake tomography. Stations located along the main profile were conceived for receiver function analysis (Zhao et al., 2015). Their spacing ranges from ~5 km in the Western Alps mountain range to ~10 km in the European foreland and in the western Po Plain. Off profile stations were installed to improve the crossing of seismic rays for local earthquake tomography.

The high number of recording stations along the main CIFALPS profile may increase the computational burden during local earthquake tomography (e.g. in ray tracing) without a direct improvement in the final resolution. However, it ensures a number of advantages. For example, any

potential loss of data due to station malfunctioning is easily recovered by adjacent instruments, and doubtful data can be discarded without jeopardizing the quality of the dataset. In order to improve the ray coverage and ensure ray crossing from any azimuth in the study volume, we added to the dataset all published phase pickings recorded by permanent seismic stations operating in France and Italy during the CIFALPS experiment (red marks in Figure 1B). We additionally considered few events that occurred before the experiment to fill specific spatial gaps. This was the case of the intermediate depth earthquakes that were useful to sample anomalies at the bottom of the study volume. Because these earthquakes are relatively rare (Eva et al., 2015), only few events were recorded during the CIFALPS experiment. In summary, 270 events on a total of 1088 events utilized in this work were added as supplementary entries from datasets available at French and Italian seismic networks; about 80% of the remaining events were merged with existing phase pickings. The final P and S ray coverage is shown in Figure 2A.

3.2. Seismic tomography setup and reconstruction test

We adopted the local earhquake tomography code SIMULPS (Thurber, 1983) for tomographic analysis, in its version 14 that implements the ray tracer by Virieux (1991) to cope with models of regional size. We subdivided the study volume into layers containing nodes, and used an initial velocity model derived from previous seismic experiments over a larger area (Scafidi et al., 2009). Several tests were performed for a correct choice of the inversion parameters, and classical damping trade-off curves (Eberhart-Phillips, 1986) were computed to pick up the best values for P and S velocities.

The resolution capability of the coupling between inversion setup and data was evaluated by checkerboard and reconstruction tests. These tests were useful to choose an adequate geometry of the starting model and evaluate the smearing due to the contrast between high and low velocity anomalies. The reconstruction test was specifically conceived to test the potential impact of the high-velocity Ivrea body, a long recognized tectonic feature associated to a positive gravimetric

anomaly (red dotted line in Fig. 1) and interpreted as a slice of Adriatic mantle emplaced at shallow depth (Closs and Labrouste, 1963; Nicolas et al., 1990). We used a “stairwell” geometry to simulate a high-velocity east-dipping layer along the CIFALPS profile (Fig. 2B) and test the resolution capability of the coupling between seismic dataset and inversion setup. The same geometry after interpolation by the algorithm used in SIMULPS is shown in Figure 2C. A comparison with Figure 2B shows that the interpolation process introduces a smoothing of the anomalies and a band of fake colors around them. Figure 2D shows the reconstruction of the imposed stairwell structure based on our seismic dataset. The inversion of synthetic data does not consider the resolution, and Figure 2D only displays the reconstructed model as if it was completely resolved except for areas that were not sampled (in white). As shown in the reconstruction test, the shape of the anomaly is well reproduced, but the velocity of the first and second steps is lowered from ~8.0 km/s (blueish) to about ~7.5 km/s (greenish), and weak vertical and horizontal periodic stripes of yellow color appear at ~50 km depth. These artifacts, and the undestimation of the magnitude of the high velocity anomalies in the uppermost 10 km of the crust, have been considered during the subsequent phases of tomography interpretation. The real data tomographic model is about 700×700 km wide, and was obtained after 6 iterations on a 12 layers model of 36×36 nodes each. In the central part of the model, spacing between nodes is equal to 15 km.

4. Results

Figure 3 shows the Vp and Vp/Vs cross-sections along the CIFALPS profile. The lighter areas are those where the diagonal elements of the resolution matrix are <0.1. This threshold was chosen as the divider between resolved and non-resolved areas based on a comprehensive comparisons between different resolution indicators (Paul et al., 2001). As expected, the maximum depth of the resolved area is limited by the depth of occurrence of most of the deepest events (Eva et al., 2015; Malusà et al., 2017). Beneath the Dora-Maira (U)HP dome, the tomography model is well resolved down to 50-60 km depth, whereas the two extremes of the CIFALPS cross section are poorly

resolved. Letters “a” to “k” indicate the relevant velocity features highlighted by the tomography model. The main tectonic structures previously inferred from receiver function analysis (Zhao et al. 2015) and surface geology (Lardeaux et al., 2006; Malusà et al., 2015) are also indicated for comparison (black lines in Fig. 3).

The most prominent feature of the tomography model is represented by the high velocity body (Vp ~7.5 km/s; Vp/Vs = 1.70-1.72), labelled with “a”, which is located right below the Dora-Maira (U)HP dome, at depths as shallow as ~10 km. Such a high-velocity body was already imaged with similar velocities by previous works (Vp ~7.4-7.7 km/s; Paul et al., 2001; Béthoux et al., 2007), but was only resolved down to depths of 15-20 km. It is still observed to the south of the CIFALPS profile (Fig. 4D,E), but progressively vanishing towards the north (Fig. 4A,B). A series of N-S cross sections, ranging from the Western Alps to the Po Plain (Fig. 5), shows that this high-velocity anomaly is exclusively found beneath the Dora-Maira (U)HP dome (Fig. 5A), and disappears farther east.

The mantle-wedge region labelled with “b” is located at depth of 20-45 km, in correspondence with a cluster of intermediate depth earthquakes and with a seismically active fault in the mantle described in previous studies (Rivoli-Marene deep fault; Eva et al., 2015; Malusà et al., 2017). This region shows higher Vp values (~8.0 km/s) compared to region “a”, and anomalously high Vp/Vs ratios (>1.74) that are supportive of low shear wave velocities. This cluster of intermediate depth earthquakes in region “b” is not only observed along the CIFALPS profile, but also in cross sections located more to the north or to the south (Fig. 4). The deepest mantle wedge region resolved by the tomographic model is labelled with “c”. This region, located at depth of ~40-50 km atop the European slab, shows lower Vp and Vp/Vs values compared to region “b” (Vp ~7.0-7.5 km/s; Vp/Vs < 1.70), but the Vp/Vs ratio is locally higher (Vp/Vs ~1.74).

The well-resolved regions of the model also include some subducted European lower crust. This shows a progressive increase in Vp from the region labelled with “d” (Vp ~6.7 km/s) to the region labelled with “e” (Vp ~7.7 km/s), under a rather constant Vp/Vs ratio of 1.70-1.72. Such variations

202 are detected in all of the analyzed WSW-ENE transects of Figure 4. No seismic event was recorded
203 in regions “d” and “e” since 1990 (installation of permanent seismic networks) and during the
204 CIFALPS experiment (Eva et al., 2015; Malusà et al., 2017).

205 On the eastern side of the transect, the region labelled with “f” is located below the Adriatic
206 Moho as determined by receiver function analysis combined with gravity modelling. It shows Vp
207 values ~8.0 km/s and Vp/Vs = 1.70-1.72. This region is affected by intermediate depth earthquakes
208 that are also observed to the north and to the south of the CIFALPS transect (Fig. 4). The vertical
209 and horizontal periodic stripes of yellow color observed at 50 km depth in this region are artifacts,
210 as confirmed by the reconstruction test of Fig. 2D. Above the Adriatic Moho, measured Vp values
211 are much lower, but very high Vp/Vs values (>1.8) are locally observed at ~30 km depth at the base
212 of the Adriatic crust. This region, labelled with “g”, is also characterized by a cluster of seismic
213 events that are only observed in the vicinity of the main CIFALPS transect.

214 In the uppermost part of the Alpine orogenic wedge (regions “h” to “k”), Vp values are
215 invariably <6.5 km/s, but major variations in Vp/Vs ratios are locally observed. For example, the
216 region to the east of the Dora-Maira (U)HP dome (labelled with “h”) shows Vp/Vs values >1.72,
217 whereas the region corresponding to the western flank of the Dora-Maira dome (labelled with “j”)
218 shows much lower Vp/Vs ratios, even <1.66. Vp/Vs ratios <1.68 are also observed in the region
219 labelled with “k”, located beneath the Frontal Pennine Fault. The double-vergence accretionary
220 wedge located to the east of the Frontal Pennine Fault, and labelled with “i”, shows instead Vp/Vs
221 values > 1.75, and includes most of the shallow earthquakes recorded in the Western Alps area.

222 **5. Comparison with receiver function analysis**

223 Results of local earthquake tomography are compared in Figure 6 with published CIFALPS
224 results of receiver function analysis (Zhao et al., 2015). Unlike local earthquake tomography, the
225 receiver function technique is based on the analysis of teleseismic earthquakes, and enhances P-to-S
226 (Ps)-converted waves on velocity interfaces beneath an array. The polarity of the converted signal

depends on the sign of the velocity change, and interfaces with velocity increase can be discriminated from interfaces with velocity decrease. Assumptions and arbitrary choices of the receiver function approach applied to the CIFALPS transect (e.g., magnitude threshold, epicentral distance, seismograms filtering, velocity model, choice of the direction of back azimuths) are described in full in Zhao et al. (2015).

The image of Figure 6B is based on radial receiver functions from teleseismic events with magnitude ≥5.5, epicentral distance of 30-90°, and ENE back-azimuths (see Zhao et al., 2015). This image shows two major interfaces marked by positive-polarity Ps-conversions (red-to-yellow regions), which attest the downward velocity increase corresponding to the European and Adriatic Mohos (thick dashed lines). The eastward-dipping European Moho is recognized from ~40 km depth beneath the Frontal Pennine Fault to ~75 km depth beneath the Po Plain. The Adriatic Moho is recognized from 20-30 km depth, to the east, to 10-15 km depth, to the west. The red spots located at 40-55 km depth beneath the Adriatic Moho are multiples, as confirmed by synthetic tests (Zhao et al., 2015). A shallow positive-polarity converted phase is also observed beneath the Dora-Maira massif, between regions “a” and “h”, whereas a spot of negative-polarity Ps-conversions marking a downward velocity decrease is located above region “c”, at 20-40 km depth (blue region).

On the eastern side of the CIFALPS transect, the sharp velocity increase from Vp <6.5 km/s to Vp >8 km/s evidenced by local earthquake tomography faithfully matches the location of the downward velocity increase highlighted by receiver function analysis. Localized anomalies in Vp/Vs ratios, e.g., in region “g”, match with major breaks in the alignment of positive-polarity Ps-conversions. Beneath the Dora-Maira (U)HP dome, the downward increase in Vp values from region “h” (Vp <6.5 km/s) to region “a” (Vp ~7.5 km/s) is consistent with the observed positive-polarity Ps-conversions, whereas the downward velocity decrease from regions “a” and “b” (Vp ~7.5 km/s and >8 km/s) to region “c” (Vp ~7.0-7.5 km/s) is consistent with the spot of negative-polarity Ps-conversions located at 20-40 km depth in Figure 6B. The shape of the high-velocity

253 region labelled with “a” is also mirrored by the distribution of seismic events recorded since 1990.
254 Region “a” is virtually aseismic (Malusà et al., 2017), and earthquakes are chiefly located along its
255 external boundaries or in the surrounding regions (Fig. 6B). On the western side of the CIFALPS
256 transect, the alignment of positive-polarity Ps-conversions generated along the European Moho is
257 partly included within the resolved area of the local earthquake tomography model, and fits with a
258 downward velocity increase from ~6.7 km/s (region “d”) to >8 km/s. The velocity structure
259 unravelled by the analysis of local earthquakes is thus independently confirmed by the analysis of
260 teleseismic earthquakes (Zhao et al., 2015) and by the distribution of seismic events (Eva et al.,
261 2015; Malusà et al., 2017).

262 **6. Geologic interpretation**

263 The geologic cross section of Figure 6C shows the main features of the orogenic wedge of the
264 Western Alps, and of the mantle wedge between the European and the Adriatic plates as inferred
265 from the velocity structure derived from local earthquake tomography along the CIFALPS profile.
266 In the European plate, the Vp increase evidenced at ~40 km depth by local earthquake tomography,
267 from <6.5 km/s in region “d” to >8 km/s in region “e”, is consistent with a progressive
268 eclogitization of the lower crust and consequent density increase by metamorphic phase changes
269 (e.g., Hacker et al., 2003). This interpretation also explains the progressive weakening of the
270 positive-polarity converted phases observed along the European Moho (from red to yellow
271 background colours in Fig. 6B) previously described by Zhao et al. (2015). In more detail, the
272 velocity of the European lower crust is symptomatic of an intermediate granulitic composition in its
273 western part (e.g. Weiss et al., 1999; Wang et al., 2005), and of a progressive increase in garnet
274 content to the east during transition from granulite to eclogite (Christensen, 1989; Hacker et al.,
275 2003). Observed Vp values in this region are far too low for a pure mafic eclogite (Bezacier et al.
276 2010; Reynard, 2013), thus suggesting no compositional change from west to east in the European
277 lower crust, but only an increase in metamorphic grade. This interpretation is consistent with the

278 progressive increase in Vs values from west to east described along the same transect (Lyu et al.,
279 2017).

280 On the eastern side of the Western Alps, Vp values >8 km/s confirm the presence of Adriatic
281 mantle at shallow depth beneath the western Po Plain (10-15 km), just in correspondence with the
282 positive gravimetric anomaly classically referred to as the Ivrea body (Closs and Labrouste, 1963;
283 Nicolas et al., 1990) and in line with results of previous tomographic models (e.g., Solarino et al.
284 1997; Paul et al., 2001; Scafidi et al., 2006; 2009; Diehl et al., 2009; Wagner et al., 2012). East of
285 the Ivrea body gravimetric anomaly, the Adriatic Moho is located at 30-35 km depth, which is a
286 much more reliable estimate of the Moho depth beneath the Po Plain compared to previous
287 estimates based on receiver function alone (Zhao et al. , 2015). The locally high Vp/Vs ratios >1.8,
288 associated to Vp of 7.0-7.5 km/s (region “g”), may be supportive of gabbro (Weiss et al., 1999)
289 underplated at the base of the Adriatic lower crust. Noteworthy, Permian gabbros are indeed
290 exposed north of the Po plain, where they are intruded into lower crust rocks belonging to the
291 Adriatic (Southalpine) basement (Quick et al., 1994; Schaltegger and Brack, 2007).

292 In the uppermost part of the Alpine wedge, the structural variability of stacked rocks is largely
293 mirrored by their variability in Vp/Vs ratios. The Vp/Vs values >1.75 observed in the double-
294 vergence accretionary wedge, chiefly including Briançonnais and Schistes lustrés units (Lardeaux et
295 al., 2006; Malusà et al., 2015), may reflect low Vs values, possibly associated to the widespread
296 network of mesoscale faults developed in these rocks since the Neogene (Tricart et al., 2004; Sue et
297 al., 2007; Malusà et al., 2009). To the east, low Vp/Vs values even <1.66 observed on the western
298 flank of the Dora-Maira dome (region “j”) may instead reflect high Vs velocities, suggesting that
299 the poorly fractured granitic gneisses exposed at the surface (Brossasco granite; Paquette et al.,
300 1999; Lenze and Stöckhert, 2007) may be also present at depth. Fracturing may be also invoked to
301 explain the low Vs values observed along the eastern boundary of the Dora-Maira dome, where
302 (U)HP continental rocks are juxtaposed against the eclogitized mantle rocks of the Lanzo massif
303 (Kienast and Pognante, 1988; Piccardo et al., 2007) along the Lis-Trana deformation zone (Perrone

et al., 2010). To the west of the Frontal Pennine Fault, Vp/Vs values <1.68 suggest instead that the European upper crust in the External zones is poorly deformed, consistent with minor seismicity recorded in that area (Fig. 6B).

But the most relevant information provided by the tomography model presented in this article is related to the velocity structure beneath the Dora-Maira (U)HP dome. Two end-member tectonic reconstructions were recently proposed for this region in the light of available geophysical data (Zhao et al., 2015; Malusà et al., 2017): one invoking a thick complex of (U)HP continental slivers, in line with the predictions of numerical models of syn-convergent exhumation (e.g., Butler et al., 2013; Jamieson and Beaumont, 2013), and another one invoking a larger volume of mantle rocks exhumed at shallow depth during divergence between the upper plate and the accretionary wedge (e.g., Malusà et al., 2011, 2015). Our tomographic model can be used to discriminate between these end-member hypotheses.

The velocity structure of the mantle wedge region “a”, showing Vp velocity of ~7.5 km/s from depths as shallow as ~10 km down to ~30 km, is largely inconsistent with the presence of dry mantle peridotite beneath the Dora-Maira (U)HP continental rocks, and suggests a complex history for these rocks in terms of P-T conditions and fluid-rock interaction. Such Vp values point in fact to widespread serpentinization of mantle rocks (~60% according to Reynard, 2013), that may locally exceed 90% both in the uppermost part of anomaly “a” and in the Lanzo massif, although velocity values in the uppermost crustal levels may be slightly underestimated as unravelled by the reconstruction tests of Fig. 2D. The degree of serpentinization at 30-40 km depth is instead much lower (<30%), and consistent with the occurrence of intermediate-depth earthquakes (Fig. 6B). Vp/Vs ratios are in the range of 1.70-1.72 in region “a”, but sharply increase to values >1.74 in region “b”, where Vp values (~8.0 km/s) are consistent with dry mantle peridotite. The high Vp/Vs ratios in region “b” point to low shear wave velocities, which are in line with the presence of a major active fault in the upper mantle as underlined by the alignment of anomalously deep earthquakes (Eva et al., 2015). According to previous work, the deepest part of the mantle wedge

beneath the thick blue spot of negative polarity conversions (region “c” in Fig. 6B) may either include serpentinites, or slivers of (U)HP rocks. Our results indicate that the velocity values observed in region “c” (Vp ~7.0-7.5 km/s; Vp/Vs <1.70) are neither consistent with eclogitic metasediments (Vp ~7.0 km/s; Vp/Vs ~1.75) nor with mafic eclogite (Vp > 8.0 Vp/Vs ~1,73), but are instead supportive of ultramafic rocks with a degree of serpentinization ranging between 50% and 75% (Reynard, 2013). Minor slivers of eclogitic metasediments may be present beneath the mantle wedge, in regions showing the highest Vp/Vs ratios at the top of the European slab. These results demonstrate that recent geologic cross-sections postulating a thick wedge of Briançonnais eclogites beneath the Dora-Maira (Schmid et al., 2017) are likely incorrect, and that the palinspastic reconstruction of the Alps-Apennines transition zone derived from such geologic cross-sections should be reconsidered.

7. Implication for (U)HP rock exhumation

In the southern Western Alps, the positive gravimetric anomaly ascribed to the Ivrea body is classically interpreted in terms of upper mantle indentation (e.g., Lardeaux et al., 2006; Béthoux et al., 2007), in line with previous tectonic interpretations proposed for the Central Alps and for the northern Western Alps (Schmid and Kissling, 2000). According to these interpretations, the uppermost part of the Adriatic mantle would act as an indenter beneath the Alpine accretionary wedge, and would transfer compression towards the European foreland. The main geologic implications of this model include: (i) major crustal shortening in the upper plate, and (ii) fast erosion focused above the indenter (Fig. 7A). These features are indeed observed in the Central Alps, where upper mantle indentation accommodated by back-folding of (U)HP domes (Keller et al., 2005) and by backthrusting of Adriatic units (Zanchetta et al., 2015) triggered the fast erosional exhumation of the amphibolite-facies Lepontine dome (Malusà et al., 2016). However, these features are not common to the southern Western Alps. Indeed, during and after Eocene (U)HP rock exhumation, shortening recorded in the accretionary wedge of the southern Western Alps was minor

(Malusà et al., 2009; Dumont et al., 2012) and erosion was much slower compared to the Lepontine dome, as attested by low-temperature thermochronometers (Vernon et al., 2008; Fox et al., 2015) and by preserved Oligocene corals unconformably lying on top of Eocene eclogites (Quaranta et al. 2009; Malusà et al., 2015). A tectonic scenario exclusively invoking upper-plate mantle indentation beneath the accretionary wedge would also imply that seismic velocities in the mantle of the upper plate should be quite similar beneath the orogenic wedge and in the hinterland (Fig. 7A). Major seismic velocity changes, e.g., by metamorphic phase changes triggered by fluids released by the downgoing slab, would remain probably undetected in the local earthquake tomography model, because they would take place at much greater depth (Deschamps et al., 2013; Abers et al., 2017).

Noteworthy, our study points to a complex velocity structure in the upper plate mantle of the southern Western Alps. The region beneath the Dora-Maira (U)HP dome is dominated by serpentinized peridotites, documented from ~10 km depth down to the top of the European slab. To the east, these rocks are juxtaposed against dry mantle peridotites of the Adriatic upper plate along a steeply dipping fault in the lithospheric mantle. In between, mantle rocks of the Lanzo massif underwent subduction during the Alpine orogeny, and were later exhumed and accreted against the Adriatic upper plate when the Dora-Maira (U)HP rocks were still buried at mantle depths (Rubatto and Hermann, 2001). This scenario may suggest (U)HP rock and mantle-wedge exhumation mainly triggered by upper plate divergent motion (Fig. 7B). Serpentinized peridotites with Vp ~7.5 km/s that are found beneath the Dora-Maira dome may have favoured the exhumation of (U)HP rocks across the upper crust, where these rocks become neutrally buoyant (e.g., Schwartz et al., 2001). No exhumed mantle-wedge serpentinites are recognized so far at outcrop in the southern Western Alps (Scambelluri et al., 1995; Piccardo et al., 2004; Hattori and Guillot, 2007; Deschamps et al., 2013). However strong fluid-rock interactions are recognized in subducted serpentinites and associated ophiolitic rocks (Scambelluri and Tonarini, 2012; Lafay et al., 2013; Plümber et al., 2017), suggesting that fluid release may have occurred during oceanic and even during continental subduction (e.g., Castelli et al., 2007; Ferrando et al., 2009) possibly triggering the partial

serpentinization of the Adriatic mantle wedge. Part of the Adriatic mantle wedge was then exhumed at shallow crustal levels during late Eocene transtension along the Western Alps subduction zone (Malusà et al. 2015), and was finally indented beneath the Alpine wedge during the early Oligocene tectonic shortening (Dumont et al., 2012; Jourdan et al., 2012, 2013). Along the Adria-Europe plate boundary, the divergent component of Eocene transtension progressively decreased towards the north to become negligible in the Central Alps, where Adria was indented more deeply beneath the accretionary wedge compared to the Western Alps (Malusà et al., 2015). We speculate that, north of the Dora-Maira dome, upper plate divergence was probably insufficient to allow an effective exhumation of the mantle wedge. However, testing this hypothesis would require a high resolution tomographic image of the northern Western Alps, which may be precluded by the lack of deep earthquakes.

The occurrence of mantle-wedge serpentinites exhumed at shallow depth within a continental subduction zone is not specific of the southern Western Alps. Mantle wedge serpentinites associated with (U)HP rock are described, for example, in the Indus Suture Zone in the Himalaya, in the Carribbean (Guillot et al., 2001; Deschamps et al., 2012), in the Western Gneiss Region in Norway (Scambelluri et al., 2010), and are inferred by geophysical evidence under the Dabie-Sulu (Liu et al., 2015). Our findings suggest that orogen-scale exhumation of the mantle wedge may represent a prominent, but still underestimated feature of the deep structure of many orogenic belts. As such, it should be integrated in more advanced theoretical models of subduction and exhumation. Moreover, widespread mantle-wedge exhumation may explain the common occurrence of boudinaged mantle-wedge rocks within continental UHP rocks in the roots of old orogenic belts now unroofed by erosion. In pre-Cenozoic orogenic belts such as the Dabie-Sulu or the Western Gneiss Region, where the evidence of minor erosion during UHP exhumation, if any, is no longer preserved, the occurrence of mantle wedge rocks at shallow depth may represent the only evidence supporting (U)HP rock exhumation triggered by divergent motion between upper plate and accretionary wedge.

8. Conclusions

The new local earthquake tomography model of the southern Western Alps, independently validated by receiver function analysis, unravels a complex seismic velocity pattern consistent with a composite structure of the mantle wedge above the subducted European lithosphere. Seismic velocities indicate that the Dora-Maira (U)HP dome lays directly above serpentinized peridotites, documented from ~10 km depth down to the top of the eclogitized lower crust of the European plate. We propose that peridotite serpentinization was the result of fluids released to the Adriatic mantle wedge during Alpine subduction. The minor amount of eclogitic metasediments above the European slab indicates that the subduction wedge was largely exhumed during Eocene transtension, when part of the mantle wedge was also exhumed at shallow crustal levels to be finally indented under the Alpine metamorphic units. The serpentinized peridotites imaged beneath the Dora-Maira (U)HP dome are not exposed at Earth's surface, and are juxtaposed against dry mantle peridotites of the Adriatic upper plate along an active fault rooted in the lithospheric mantle. Our results suggest that mantle wedge exhumation may represent an important feature of the deep structure of exhumed continental subduction zones. Deep orogenic levels as those imaged by local earthquake tomography in the southern Western Alps may be exposed today in older continental subduction zones, where mantle wedge serpentinites are commonly associated to continental (U)HP metamorphic rocks.

Acknowledgments. This work is funded by the State Key Laboratory of Lithospheric Evolution, China, the National Natural Science Foundation of China (Grant 41350001), and a grant from LabEx OSUG@2020 (Investissements d'avenir; ANR10 LABX56, France). The earthquake waveforms used in this study are available at the European Integrated Data Archive (eida.rm.ingv.it) (see also doi:10.13127/SD/X0FXnH7QfY; doi:10.12686/sed/networks/2a). The CIFALPS seismic data are archived at the data center of the Seismic Array Laboratory, Institute of Geology and Geophysics, Chinese Academy of Sciences, and at the data center of the French Seismologic and Geodetic Network RESIF (doi:10.15778/RESIF.YP2012). The manuscript benefited from insightful discussions with S. Baldwin, S. Ferrando and N. Malaspina.

References

Abers, G. A., van Keken, P. E., Hacker, B. R., 2017. The cold and relatively dry nature of mantle forearcs in subduction zones. Nature Geoscience 10(5), 333-337.

Agard, P., Monie, P., Jolivet, L., Goffé, B., 2002. Exhumation of the Schistes Lustrés complex: In situ laser probe Ar-40/Ar-39 constraints and implications for the western Alps. Journal of Metamorphic Geology 20, 599–618.

Agard, P., Yamato, P., Jolivet, L., Burov, E., 2009. Exhumation of oceanic blueschists and eclogites in subduction zones: timing and mechanisms. Earth-Science Reviews 92(1), 53-79.

Angiboust, S., Langdon, R., Agard, P., Waters, D. J., Chopin, C. 2012. Eclogitization of the Monviso ophiolite (W Alps) and implications on subduction dynamics. Journal of Metamorphic Geology 30, 37–61.

Avigad, D., Chopin, C., Le Bayon, R., 2003. Thrusting and extension in the southern Dora-Maira ultra-high-pressure massif (Western Alps): view from below the coesite-bearing unit. The Journal of geology 111(1), 57-70.

Ballèvre, M., Lagabrielle, Y., Merle, O., 1990. Tertiary ductile normal faulting as a consequence of lithospheric stacking in the western Alps. Société Géologique de France, Mémoires 156, 227–236.

Béthoux, N., Sue, C., Paul, A., Virieux, J., Fréchet, J., Thouvenot, F., Cattaneo, M., 2007. Local tomography and focal mechanisms in the south-western Alps: comparison of methods and tectonic implications. Tectonophysics 432, 1–19.

Bezacier, L., Reynard, B., Bass, J.D., Wang, J., Mainprice, D., 2010. Elasticity of glaucophane, seismic velocities and anisotropy of the subducted oceanic crust. Tectonophysics 494, 201–210.

Blake, M.C., Jayko, A.S., 1990. Uplift of very high pressure rocks in the western Alps: Evidence for structural attenuation along low angle faults. In: Roure, F., Heitzmann, P., Polino, R. (Eds.), Deep structure of the Alps. Mémoire de la Société Géologique de France 156, pp. 228–237.

Boudier, F., 1978. Structure and petrology of the Lanzo peridotite massif (Piedmont Alps). Geological Society of America Bulletin 89(10), 1574-1591.

Butler, J.P., Beaumont, C., Jamieson, R.A., 2013. The Alps 1: A working geodynamic model for burial and exhumation of (ultra) high-pressure rocks in Alpine-type orogens. Earth and Planetary Science Letters 377, 114–131.

Carswell, D. A., R. Compagnoni (Eds.), 2003. Ultrahigh Pressure Metamorphism, 508 pp., Eotvos Univ. Press, Budapest.

Castelli, D., Rolfo, F., Groppo, C., Compagnoni, R., 2007. Impure marbles from the UHP Brossasco-Isasca Unit (Dora-Maira Massif, western Alps): evidence for Alpine equilibration in the diamond stability field and evaluation of the X(CO_2) fluid evolution Journal of Metamorphic Geology, 25, 587-603

Chopin, C., 1984. Coesite and pure pyrope in high-grade blueschists of the Western Alps: A first record and some consequences. Contributions to Mineralogy and Petrology 86, 107–118.

Chopin, C., Henry, C., Michard, A., 1991. Geology and petrology of the coesite bearing terrain, Dora-Maira massif, western Alps. European Journal of Mineralogy 3, 263–291.

Christensen, N.I., 1989. Seismic velocities. In: Carmichael, R.S. (Ed.), Practical Handbookof Physical Properties of Rocks and Minerals. CRC Press, Boca Raton, p. 741

Closs, H. and Labrouste Y. (Eds.), 1963. Rechèrches séismologiques dans les Alpes occidentales au moyen de grandes explosions en 1956, 1958 et 1960. Mem. Coll. Année Geophys. Int. 12-2. CNRS Paris, 241 pp.

Compagnoni, R., Rolfo, F., 2003. UHPM units in the western Alps: European Mineralogy Union Notes in Mineralogy 5, 13–49.

Coward, M., Dietrich, D., 1989. Alpine tectonics: an overview. In: Coward, M., Dietrich, D., Park, R.G. (Eds), Alpine Tectonics. Geological Society, London, Special Publications 45, pp. 1–29.

Debret, B., Nicollet, C., Andreani, M, Schwartz, S., Godard, M., 2013. Three steps of serpentinization in an eclogitised oceanic serpentinisation front (Lanzo massif - Western Alps). Journal of Metamorphic Geology 31, 165–186.

Deschamps, F., Godard, M., Guillot, S., Chauvel, C., Andreani, M., Hattori K., Wunder B., France L., 2012. Behavior of fluid-mobile elements in serpentines from abyssal to subduction environments: Examples from Cuba and Dominican Republic. Chemical Geology 313, 93–117.

Deschamps, F., Godard, M., Guillot, S., Hattori, K.H., 2013. Geochemistry of subduction zone serpentinites: A review. Lithos 178, 96-127.

Diehl, T., Husen, S., Kissling, E., Deichmann, N., 2009. High-resolution 3-D P-wave model of the Alpine crust. Geophysical Journal International 179(2), 1133–1147.

Duchêne, S., Blichert-Toft, J., Luais, B., Télouk, P., Lardeaux, J.M., and Albarède, F., 1997. The Lu-Hf dating of garnets and the ages of the Alpine high-pressure metamorphism. Nature 387, 586–589.

Dumont, T., Schwartz, S., Guillot, S., Simon-Labric, T., Tricart, P., Jourdan, S., 2012. Structural and sedimentary records of the Oligocene revolution in the Western Alps. Journal of Geodynamics 56, 18–38.

Eberhart-Phillips, D., 1986. Three-dimensional velocity structure in northern California Coast Ranges from inversion of local earthquake arrival times. Bulletin of the Seismological Society of America 76(4), 1025–1052.

Eva, E., Malusà, M.G., Solarino, S., 2015. A seismotectonic picture of the inner southern Western Alps based on the analysis of anomalously deep earthquakes. Tectonophysics 661, 190–199.

Ferrando, S., Frezzotti, M. L., Petrelli, M., Compagnoni, R., 2009. Metasomatism of continental crust during subduction: the UHP whiteschists from the Southern Dora-Maira Massif (Italian Western Alps). Journal of Metamorphic Geology 27(9), 739-756.

Ford, M., Duchêne, S., Gasquet, D., Vanderhaeghe, O., 2006. Two-phase orogenic convergence in the external and internal SW Alps. Journal of the Geological Society 163, 815–826.

Fox, M., Herman, F., Kissling, E., Willett, S.D., 2015, Rapid exhumation in the Western Alps driven by slab detachment and glacial erosion. Geology, 43, 379–382.

Ganne, J., Bertrand, J.M., Fudral, S., Marquer, D., Vidal, O., 2007. Structural and metamorphic evolution of the Ambin massif (western Alps): toward a new alternative exhumation model for the Briançonnais domain. Bulletin de la Société Géologique de France 178, 437–458.

Gilotti, J. A., 2013. The realm of ultrahigh-pressure metamorphism. Elements 9, 255–260.

Guillot, S., Hattori, K.H., de Sigoyer, J., Nägler, T., Auzende, A.L., 2001. Evidence of hydration of the mantle wedge and its role in the exhumation of eclogites. Earth and Planetary Science Letters 193, 115–127.

Guillot, S., Hattori, K., Agard, P., Schwartz, S., Vidal, O., 2009. Exhumation Processes in Oceanic and Continental Subduction Contexts: A Review, Springer, Berlin.

Hacker, B.R., Abers, G.A, Peacock, S.M., 2003. Subduction factory 1. Theoretical mineralogy, densities, seismic wave speeds, and H_2O contents. Journal of Geophysical Research: Solid Earth 108 (B1).

Hacker, B.R., McClelland, W.C., Liou J.G. (Eds.), 2006. Ultrahigh-pressure metamorphism: Deep continental subduction, Special Paper Geological Society of America 403, 206 pp.

Handy, M.R., Schmid, S.M., Bousquet, R., Kissling, E., Bernoulli, D., 2010. Reconciling plate-tectonic reconstructions of Alpine Tethys with the geological–geophysical record of spreading and subduction in the Alps. Earth-Science Reviews 102(3), 121-158.

Hattori, K.H., Guillot, S., 2007. Geochemical character of serpentinites associated with high- to ultrahigh-pressure metamorphic rocks in the Alps, Cuba, and the Himalayas: Recycling of elements in subduction zones, Geochemistry, Geophysics, Geosystems 8, Q09010, doi:10.1029/2007GC001594.

Henry, C., Michard, A., Chopin, C., 1993. Geometry and structural evolution of ultra-high pressure and high-pressure rocks from the Dora-Maira massif, western Alps, Italy. Journal of Structural Geology 15, 965–981.

Jamieson, R.A., Beaumont, C., 2013. On the origin of orogens. Geological Society of America Bulletin 125(11-12), 1671–1702.

Jourdan, S., Bernet, M., Schwartz, S., Guillot, S., Tricart, P., Chauvel, C., Dumont, T., Montagnac, G., Bureau, S., 2012. Tracing the Oligocene-Miocene evolution of the Western Alps drainage divide with pebble petrology, geochemistry, and Raman spectroscopy of foreland basin deposits. Journal of Geology 120(6), 603–624.

Jourdan, S., Bernet, M., Tricart, P., Hardwick, E., Paquette, J. L., Guillot, S., Dumont, T., Schwartz, S., 2013. Short-lived, fast erosional exhumation of the internal western Alps during the late early Oligocene: Constraints from geothermochronology of pro-and retro-side foreland basin sediments, Lithosphere 5(2), 211–225.

Keller, L.M., Hess, M., Fügenschuh, B., Schmid, S.M., 2005. Structural and metamorphic evolution of the Camughera–Moncucco, Antrona and Monte Rosa units southwest of the Simplon line, Western Alps. Eclogae Geologicae Helvetiae 98(1), 19-49.

Kienast, J.R., Pognante, U., 1988. Chloritoid-bearing assemblages in eclogitised metagabbros of the Lanzo peridotite body (western Italian Alps). Lithos 21(1), 1–11.

Lafay, R., Deschamps, F., Schwartz, S., Guillot, S., Godard, M., Nicollet, C. 2013. High pressure serpentinites, a trap and release system controlled by metamorphic conditions: Example from the Piedmont zone of the western Alps. Chemical Geology 343, 38–54.

Lagabrielle, Y., Cannat, M., 1990. Alpine jurassic ophiolites resemble the modern central atlantic basement. Geology 18, 319–322.

Lanari, P., Rolland, Y., Schwartz, S., Vidal, O. Guillot, S., Tricart, P., Dumont, T., 2014. P-T-t estimation of deformation in low-grade quartz-feldspar bearing rocks using thermodynamic modeling and $^{40}Ar/^{39}Ar$ dating techniques: example of the Plan-de-Phasy shear zone unit (Briançonnais Zone, Western Alps). Terra Nova 26, 130–138.

Lardeaux, J.M., Schwartz, S., Tricart, P., Paul, A., Guillot, S., Béthoux, N., Masson, F., 2006. A crustal-scale cross-section of the south-western Alps combining geophysical and geological imagery. Terra Nova 18, 6, 412–422.

Lemoine, M., Bas, T., Arnaud-Vanneau, A., Arnaud, H., Dumont, T., Gidon, M., Bourbon, M., De Graciansky, P.C., Rudckiewicz, J.L., Megard-Galli, J., Tricart, P., 1986. The continental margin of the Mesozoic Tethys in the Western Alps. Marine Petroleum Geology 3, 179–199.

Lenze, A., Stöckhert, B., 2007. Microfabrics of UHP metamorphic granites in the Dora Maira Massif, western Alps – no evidence of deformation at great depth. Journal of Metamorphic Geology 25(4), 461–475.

Liou, J. G., Ernst, W. G., Zhang, R. Y., Tsujimori, T., Jahn, B. M., 2009. Ultrahigh-pressure minerals and metamorphic terranes–the view from China. Journal of Asian Earth Sciences 35(3), 199-231.

Little, T. A., Hacker, B. R., Gordon, S. M., Baldwin, S. L., Fitzgerald, P. G., Ellis, S., Korchinski, M., 2011. Diapiric exhumation of Earth's youngest (UHP) eclogites in the gneiss domes of the D'Entrecasteaux Islands, Papua New Guinea. Tectonophysics 510(1), 39-68.

Liu, Y.H., Yang, H.,J., Takazawa, E., Satish-Kumar, M., You, C.F., 2015. Decoupling of the Lu-Hf, Sm-Nd, and Rb-Sr isotope systems in eclogites and a garnetite from the Sulu ultra-high pressure metamorphic terrane: Causes and implications. Lithos 234, 1–14.

571 Lombardo, B., Nervo, R., Compagnoni, R., Messiga, B., Kienast, J.R., Mével, C., Fiora, L., Piccardo, G.B.,
572 Lanza, R., 1978, Osservazioni preliminari sulle ofiolite metamorfiche del Monviso (Alpi Occidentali).
573 Rendiconti della Società Italiana di Mineralogia e Petrologia 34, 253–305.

574 Lyu, C., Pedersen, H., Paul, A., Zhao, L., Solarino, S. and the CIFALPS Working Group, 2017. Shear wave
575 velocities in the upper mantle of the Western Alps: new constraints using array analysis of seismic
576 surface waves. Geophysical Journal International, doi : 10.1093/gji/ggx166.

577 Malusà, M., Mosca, P., Borghi, A., Dela Pierre, F., Polino, R., 2002. Approccio multidisciplinare per la
578 ricostruzione dell'assetto tettono-stratigrafico e dell'evoluzione metamorfico-strutturale di un settore di
579 catena orogenica: l'esempio dell'Alta Valle di Susa (Alpi occidentali). Memorie della Società
580 Geologica Italiana 57(2), 249-257.

581 Malusà, M.G., Polino, R., Martin, S., 2005. The Gran San Bernardo nappe in the Aosta valley (western
582 Alps): a composite stack of distinct continental crust units. Bulletin de la Société géologique de France
583 176(5), 417-431.

584 Malusà, M.G., Polino, R., Zattin, M., 2009. Strain partitioning in the axial NW Alps since the Oligocene.
585 Tectonics 28, TC3005, 1-26, doi:10.1029/2008TC002370.

586 Malusà, M.G., Faccenna, C., Garzanti, E., Polino, R., 2011. Divergence in subduction zones and exhumation
587 of high-pressure rocks (Eocene Western Alps). Earth and Planetary Science Letters 310, 21–32.

588 Malusà, M.G., Faccenna, C., Baldwin, S.L., Fitzgerald, P.G., Rossetti, F., Balestrieri, M.L., Danišík, M.,
589 Ellero, A., Ottria, G., Piromallo, C., 2015. Contrasting styles of (U)HP rock exhumation along the
590 Cenozoic Adria-Europe plate boundary (Western Alps, Calabria, Corsica). Geochemistry, Geophysics,
591 Geosystems 16(6), 1786–1824.

592 Malusà, M.G., Anfinson, O.A., Dafov, L.N., Stockli, D.F., 2016. Tracking Adria indentation beneath the
593 Alps by detrital zircon U-Pb geochronology: Implications for the Oligocene–Miocene dynamics of the
594 Adriatic microplate. Geology 44(2), 155-158.

595 Malusà, M.G., Zhao, L., Eva, E., Solarino, S., Paul, A., Guillot, S., Schwartz, S., Dumont, T., Aubert, C.,
596 Salimbeni, S., Pondrelli, S., Wang Q., Zhu, R., 2017. Earthquakes in the western alpine mantle wedge.
597 Gondwana Research 44, 89–95.

598 Michard, A., Chopin, C., Henry, C., 1993. Compression versus extension in the exhumation of the Dora
599 Maira coesite-bearing unit, Western Alps, Italy. Tectonophysics 221, 173–193.

600 Michard, A., Avigad, D., Goffé, B., Chopin, C., 2004. The high-pressure metamorphic front of the south
601 Western Alps (Ubaye-Maira transect, France, Italy). Schweiz. Mineral. Petrogr. Mitt. 84, 215-235.

602 Müntener, O., Pettke, T., Desmurs, L., Meier, M., Schaltegger, U., 2004. Refertilisation of mantle peridotite
603 in embryonic ocean basins: trace element and Nd isotopic evidence and implications for crust mantle
604 relationships. Earth and Planetary Science Letters 221, 293–308.

605 Nicolas, A., Hirn, A., Nicolich, R., Polino, R., 1990. Lithospheric wedging in the western Alps inferred from
606 the ECORS-CROP traverse. Geology 18, 587–590.

607 Paquette, J. L., Montel, J. M., Chopin, C., 1999. U-Th-Pb dating of the Brossasco ultrahigh-pressure
608 metagranite, Dora-Maira massif, western Alps. European journal of mineralogy 11(1), 69–77.

609 Paul, A., Cattaneo, M., Thouvenot, F., Spallarossa, D., Béthoux, N., Fréchet, J., 2001. A three-dimansional
610 crustal velocity model of the southwestern Alps from local earthquake tomography. Journal of
611 Geophysical Research 106(B9), 19367-19389.

612 Perrone, G., Eva, E., Solarino, S., Cadoppi, P., Balestro, G., Fioraso, G., Tallone, S., 2010. Seismotectonic
613 investigations in the inner Cottian Alps (Italian Western Alps): an integrated approach.
614 Tectonophysics 496(1), 1–16.

615 Petersen, K.D., Buck, W.R., 2015. Eduction, extension, and exhumation of ultrahigh-pressure rocks in
616 metamorphic core complexes due to subduction initiation. Geochemistry, Geophysics, Geosystems
617 16(8), 2564-2581.

618 Piccardo, G.B., Müntener, O., Zanetti, A., Pettke, T., 2004. Ophiolitic peridotites of the Alpine-Apennine
619 system: mantle processes and geodynamic relevance. International Geology Review 46 (12), 1119-
620 1159.

621 Piccardo, G.B., Zanetti, A., Müntener, O., 2007. Melt/peridotite interaction in the Southern Lanzo peridotite:
622 field, textural and geochemical evidence. Lithos 94(1), 181–209.

623 Plümber, O., John, T., Podladchikov, Y.Y., Vrijmoed, J.C., Scambelluri, M., 2017. Fluid escape from
624 subduction zones controlled by channel-forming reactive porosity. Nature Geoscience 10, 150-156.

625 Quaranta, F., Piazza, M., Vannucci, G., 2009. Climatic and tectonic control on the distribution of the
626 Oligocene reefs of the Tertiary Piedmont Basin (NW Italy). Italian Journal of Geosciences 128(2),
627 587–591.

628 Quick, J. E., Sinigoi, S., Mayer, A., 1994. Emplacement dynamics of a large mafic intrusion in the lower
629 crust, Ivrea-Verbano Zone, northern Italy. Journal of Geophysical Research: Solid Earth 99(B11),
630 21559-21573.

631 Reynard, B., 2013. Serpentine in active subduction zones. Lithos 178, 171–185.

632 Rubatto, D., Hermann, J., 2001. Exhumation as fast as subduction ? Geology 29(1), 3–6.

633 Rubatto, D., Hermann, J., 2003. Zircon formation during fluid circulation in eclogites (Monviso, Western
634 Alps): implications for Zr and Hf budget in subduction zones. Geochimica et Cosmochimica Acta
635 67(12), 2173–2187.

636 Rubatto, D., Müntener, O., Barnhoorn, A., Gregory, C., 2008. Dissolution-reprecipitation of zircon at low-
637 temperature high-pressure conditions (Lanzo Massif, Italy). American Mineralogist 93, 1519–1529.

638 Scafidi, D., Solarino, S., Eva, C., 2006. Structure and properties of the Ivrea body and of the Alps-Apennines
639 systems as revealed by local earthquake tomography. Bollettino Geofisica Teorica Applicata 47, 497–514.

640 Scafidi, D., Solarino, S., Eva C., 2009. P wave seismic velocity and Vp/Vs ratio beneath the Italian Peninsula
641 from local earthquake tomography. Tectonophysics 465, 1–23.

642 Scambelluri, M., Tonarini, S., 2012. Boron isotope evidence for shallow fluid transfer across subduction
643 zones by serpentinized mantle. Geology 40, 907–910.

644 Scambelluri, M., Müntener, O., Hermann, J., Piccardo, G.B., Trommsdorff, V., 1995. Subduction of water
645 into the mantle: history of an Alpine peridotite. Geology 23, 459–462

646 Scambelluri, M., Van Roermund, H. L., Pettke, T., 2010. Mantle wedge peridotites: fossil reservoirs of deep
647 subduction zone processes: inferences from high and ultrahigh-pressure rocks from Bardane (Western
648 Norway) and Ulten (Italian Alps). Lithos 120(1), 186-201.

649 Schaltegger, U., Brack, P., 2007. Crustal-scale magmatic systems during intracontinental strike-slip
650 tectonics: U, Pb and Hf isotopic constraints from Permian magmatic rocks of the Southern Alps.
651 International Journal of Earth Sciences 96(6), 1131–1151.

652 Schmid, S.M., Kissling, E., 2000. The arc of the western Alps in the light of geophysical data on deep crustal
653 structure. Tectonics 19, 62–85.

654 Schmid, S.M., Kissling, E., Diehl, T., van Hinsbergen, D., Molli, G., 2017. Ivrea mantle wedge, arc of the
655 Western Alps, and kinematic evolution of the Alps–Apennines orogenic system. Swiss Journal of
656 Geosciences. DOI 10.1007/s00015-016-0237-0

657 Schwartz, S., Lardeaux, J.M., Guillot, S., Tricart, P., 2000. Diversité du métamorphisme éclogitique dans le
658 massif ophiolitique du Monviso (Alpes occidentales, Italie). Geodinamica Acta 13, 169-188.

659 Schwartz, S., Allemand, P., Guillot, S. 2001. Numerical model of the effect of serpentinites on the
660 exhumation of eclogitic rocks: insights from the Monviso ophiolitic massif (Western Alps).
661 Tectonophysics 342, 193–206.

662 Schwartz, S., Tricart, P., Lardeaux, J.M., Guillot, S., Vidal, O. 2009. Late tectonic and metamorphic
663 evolution of the Piedmont accretionary wedge (Queyras Schistes lustrés, western Alps): Evidences for
664 tilting during Alpine collision. Geological Society of America Bulletin 121, 502–518.

Schwartz,, S., Gautheron, C., Audin, L., Dumont, T., Nomade, J., Barbarand, J., 2017. Foreland exhumation controlled by crustal thickening in the Western Alps. Geology 45(2), 139–142.

Solarino, S., Kissling, E., Sellami, S., Smriglio, G., Thouvenot, F., Granet, M., Bonjer, K.P., Slejko, D., 1997. Compilation of a recent seismicity data base of the greater Alpine region from several seismological networks and preliminary 3D tomographic results. Annals of Geophysics 40(1).

Sue, C., Delacou, B., Champagnac, J.D., Allanic, C., Tricart, P., Burkhard, M., 2007. Extensional neotectonics around the bend of the Western/Central Alps: an overview. International Journal of Earth Sciences 96(6), 1101-1129.

Thurber, C.H., 1983. Earthquake locations and three-dimensional crustal structure in the Coyote Lake area, central California. Journal of Geophysical Research: Solid Earth 88(B10), 8226–8236.

Tricart, P., Schwartz, S., 2006. A north - south section across the Queyras Schistes lustrés (Piedmont zone, Western Alps) : syncollision refolding of a subduction wedge. Eclogae Geologicae Helvetiae 9, 429–442.

Tricart, P., Schwartz, S., Sue, C., Lardeaux, J.M., 2004. Differential exhumation in the inner western Alpine arc evidenced by late normal faulting (eastern Queyras Schistes lustrés). Journal of Structural Geology 26, 1633–1645.

Vernon, A.J., van der Beek, P.A., Sinclair, H.D., Rahn, M.K., 2008. Increase in late Neogene denudation of the European Alps confirmed by analysis of a fission-track thermochronology database. Earth and Planetary Science Letters 270, 316–329.

Virieux, J., 1991. Fast and accurate ray tracing by Hamiltonian perturbation. Journal of Geophysical Research: Solid Earth 96(B1), 579–594.

Wagner, M., Kissling, E., Husen, S., 2012. Combining controlled-source seismology and local earthquake tomography to derive a 3-D crustal model of the western Alpine region. Geophysical Journal International 191(2), 789–802.

Wang, Q., Ji, S., Salisbury, M. H., Xia, B., Pan, M., Xu, Z., 2005. Pressure dependence and anisotropy of P-wave velocities in ultrahigh-pressure metamorphic rocks from the Dabie–Sulu orogenic belt (China): implications for seismic properties of subducted slabs and origin of mantle reflections. Tectonophysics 398(1), 67–99.

Warren, C.J., 2013. Exhumation of (ultra-) high-pressure terranes: Concepts and mechanisms. Solid Earth 4(1), 75–92.

Weiss, T., Siegesmund, S., Rabbel, W., Bohlen, T., Pohl, M., 1999. Seismic velocities and anisotropy of the lower continental crust. A Review. Pure Applied Geophysics 156, 97–122.

Yamato, P., Burov, E., Agard, P., Le Pourhiet, L., Jolivet, L., 2008. HP-UHP exhumation during slow continental subduction: Self-consistent thermodynamically and thermomechanically coupled model with application to the Western Alps. Earth and Planetary Science Letters 271(1), 63-74.

Zanchetta, S., Malusà, M.G., Zanchi, A., 2015. Precollisional development and Cenozoic evolution of the Southalpine retrobelt (European Alps). Lithosphere 7, 662-681.

Zhao, L., Paul, A., Guillot, S., Solarino, S., Malusà, M.G., Zheng, T., Aubert, C., Salimbeni, S., Dumont, T., Schwartz, S., Zhu, R., Wang, Q., 2015. First seismic evidence for continental subduction beneath the Western Alps. Geology 43, 815-818.

Zhao, L., Paul, A., Malusà, M.G., Xu, X., Zheng, T., Solarino, S., Guillot, S., Schwartz, S., Dumont, T., Salimbeni, S., Aubert, C., Pondrelli, S., Wang, Q., Zhu, R., 2016a. Continuity of the Alpine slab unraveled by high-resolution P wave tomography. Journal of Geophysical Research: Solid Earth 121, 8720–8737.

Zhao, L., Paul, A., Solarino S., 2016b. Seismic network YP: CIFALPS temporary experiment (China-Italy-France Alps seismic transect). RESIF - Réseau Sismologique et géodésique Français. Seismic Network. doi:10.15778/RESIF.YP2012.

Figure 1

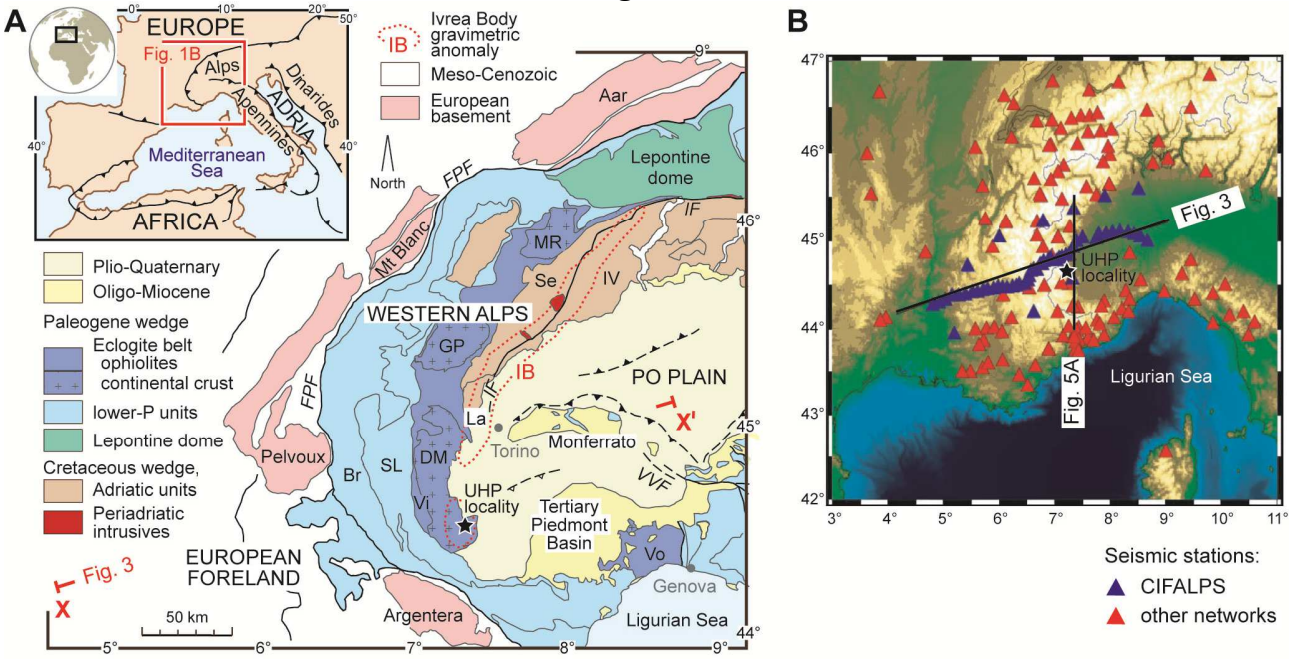

Figure 1: A) Tectonic sketch map showing the (U)HP domes of the Western Alps (dark blue), the gravimetric anomaly of the Ivrea body (0 mGal isoline in red), and the location of the CIFALPS transect (X-X'). Acronyms: Br, Briançonnais; DM, Dora-Maira; FPF, Frontal Pennine Fault; GP, Gran Paradiso; IF, Insubric Fault; IV, Ivrea-Verbano; La, Lanzo; MR, Monte Rosa; Se, Sesia-Lanzo; SL, Schistes lustrés; Vi, Viso; Vo, Voltri; VVF, Villalvernia-Varzi Fault. The black star marks the Brossasco-Isasca UHP locality. B) Seismic stations utilized in this work (blue = CIFALPS; red = other networks) and location of tomographic cross sections (black lines).

Figure 2

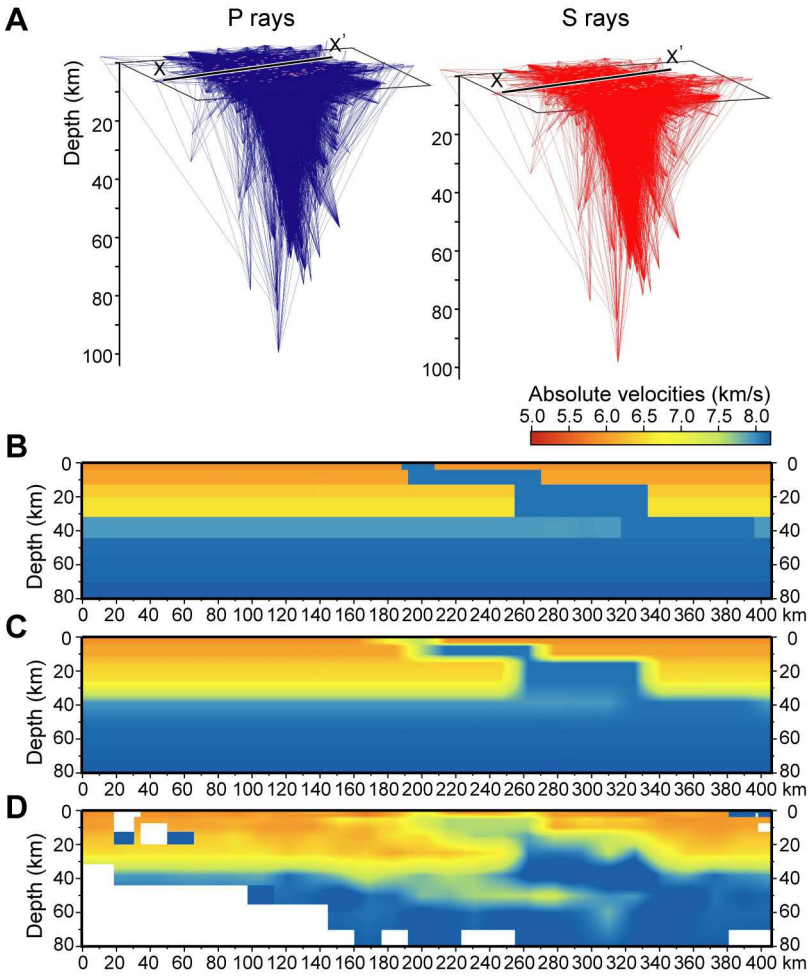

Figure 2. A) Three-dimensional P and S ray coverage based on the seismic events considered in this study (X-X' indicates the CIFALPS transect, see Fig. 1). B) Imposed stairwell geometry along the CIFALPS transect for testing the resolution capability of the coupling between seismic dataset and inversion setup. C) Same geometry after interpolation by the algorithm used in SIMULPS, which introduces a smoothing and a thin band of fake colors around the anomalies. D) Reconstruction test showing that the shape of the imposed stairwell structure is well reproduced using our dataset, but the high velocities in the uppermost 10 km are converted to lower values (as less as 0.5 km/s); the weak vertical and horizontal periodic stripes of yellow color at 50 km depth within the blue area are artifacts; white areas are not sampled.

Figure 3

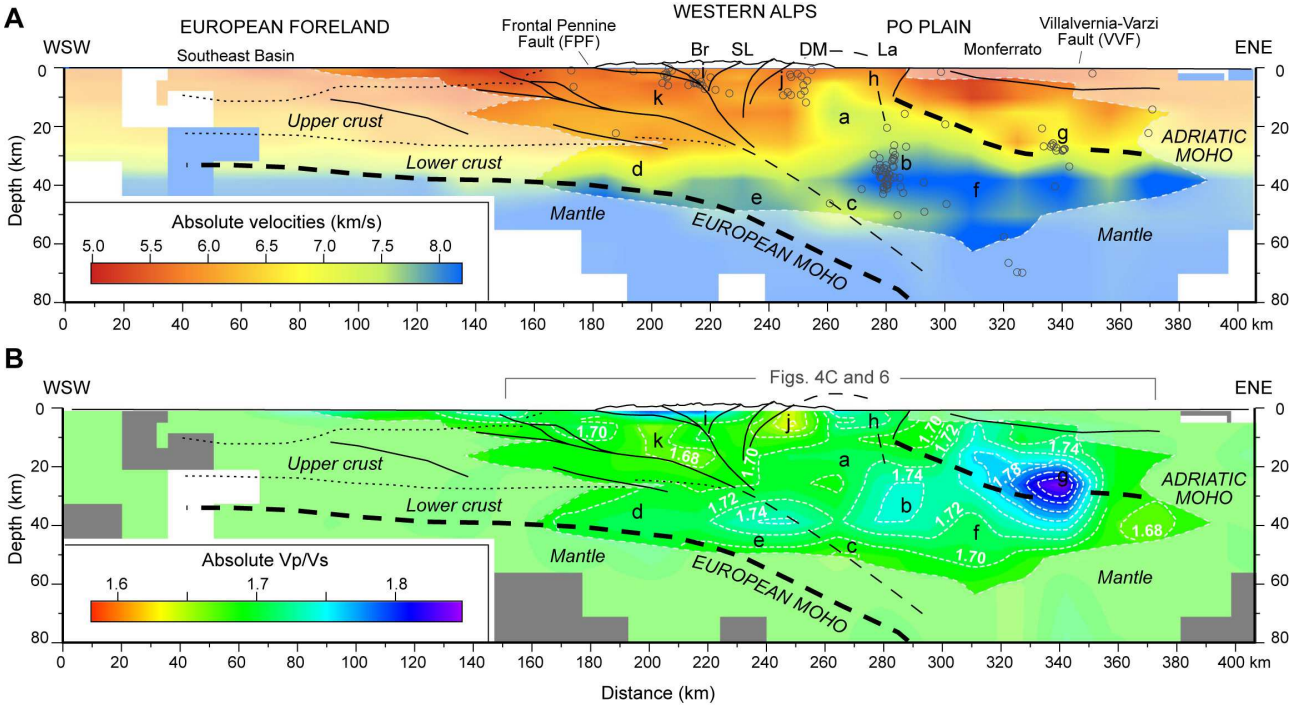

Figure 3: Tomographic cross sections along the CIFALPS transect. A) Absolute Vp velocity. The velocity structure beneath the Dora-Maira (U)HP dome is well resolved down to 50-60 km depth (acronyms as in Fig. 1A); areas with resolution diagonal elements <0.1 are masked, white areas are not sampled; letters a to k indicate regions of the model discussed in the main text; black circles indicate earthquakes as located with the 3D model; black lines and text in italics indicate the main tectonic features previously inferred from receiver function analysis (Zhao et al., 2015; Malusà et al., 2017, see Fig. 6B). Note the prominent high velocity body (labelled with "a") located right below the Dora-Maira (U)HP dome. The vertical and horizontal periodic stripes of yellow color at 50 km depth are artifacts, as attested by the reconstruction test of Fig. 2D. B) Vp/Vs ratios. White dashed lines are isolines of equal Vp/Vs, grey areas are not sampled (other keys as in frame A).

Figure 4

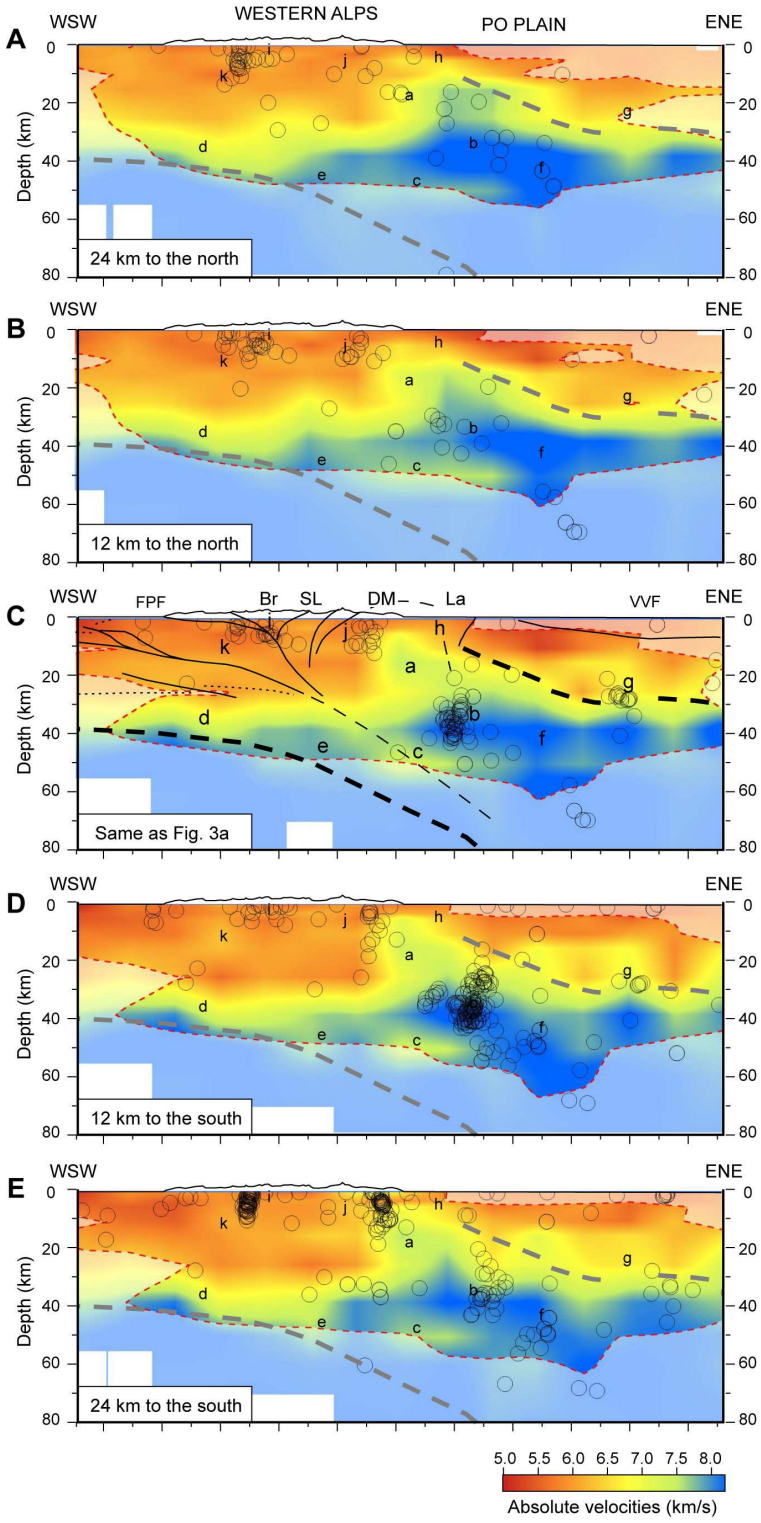

Figure 4: Lateral variations in Vp velocity in the mantle wedge as shown in a series of WSW-ENE cross-sections lying to the north (A, B) and to the south (D, E) of the main CIFALPS transect (C). The high velocity body labelled with "a" progressively disappears moving to the north. Black circles are projected hypocentres located within ±5 km distance off the profiles. The thick dashed lines, reported in all sections for comparison, indicate the European and Adriatic Mohos inferred from receiver function analysis (cf. Fig. 6B). Other keys as in Fig. 3.

Figure 5

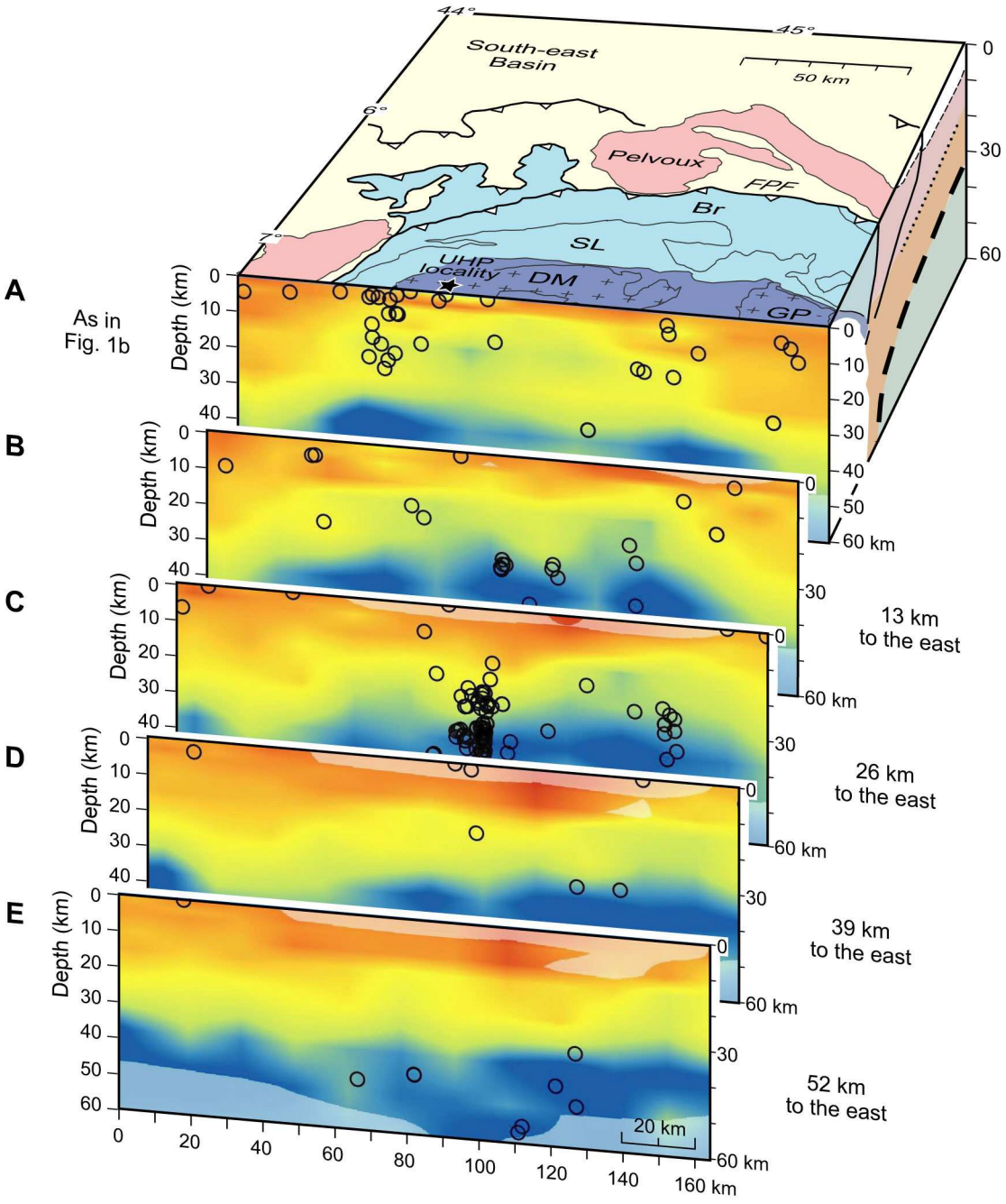

Figure 5: Lateral variations in Vp velocity beneath the Dora-Maira (U)HP dome, as shown in a series of N-S cross-sections from the mountain range to the Po Plain. Black circles are projected hypocentres located within ±3 km distance off the profiles. The high-velocity body labelled with "a" in Figs. 3 and 4 is exclusively found beneath the Dora-Maira dome (see cross section A) and progressively disappears towards the east. Acronyms as in Fig. 1.

Figure 6

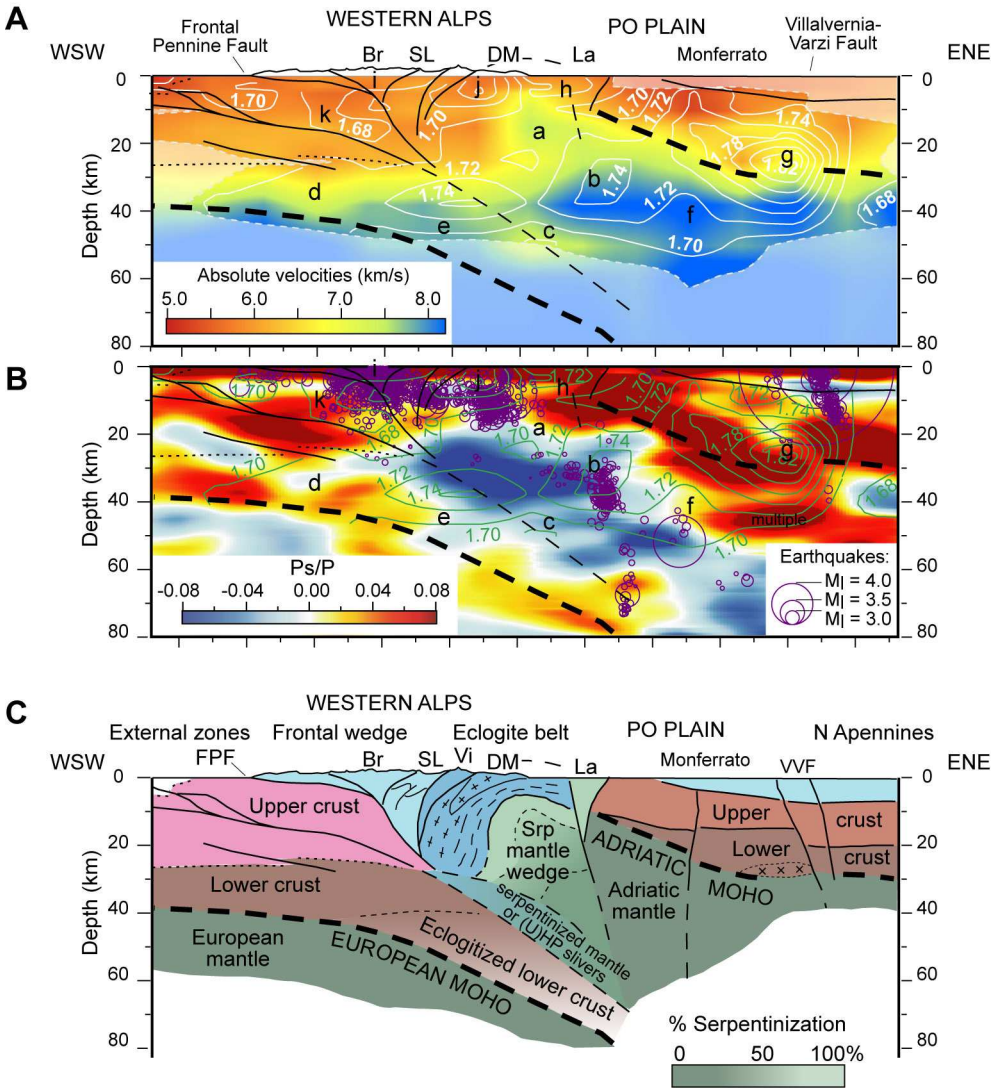

Figure 6: Synthesis of geophysical data (A, B) and inferred mantle wedge structure (C). Black lines in A and B are tectonic features based on receiver function analysis (colors in B indicate positive- and negative-polarity Ps-converted phases, Zhao et al., 2015); contours are isolines of equal Vp/Vs; purple circles in B are earthquakes recorded since 1990 (Malusà et al., 2017). The amount of serpentinization in C, in the mantle wedge underlying the Dora-Maira (U)HP dome, is inferred from seismic velocities (Reynard, 2013). Note the consistency between structures unravelled by local (A) and teleseismic (B) events. Acronyms as in Fig. 1, letters a to k as in Fig. 3.

Figure 7

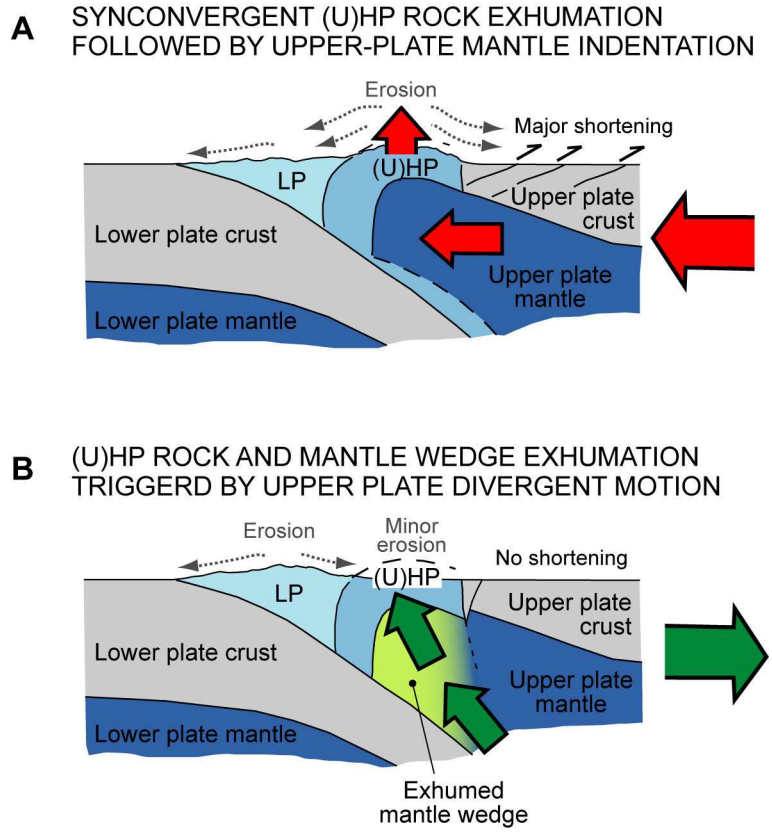

Figure 7: Alternative scenarios of mantle involvement in (U)HP orogenic belts. **A)** Synconvergent exhumation of (U)HP rocks (e.g., Butler et al., 2013) is followed by indentation of the upper-plate mantle (dark blue) beneath the accretionary wedge, with consequent fast erosion of the (U)HP dome and major tectonic shortening in the upper plate (e.g., Béthoux et al., 2007). Seismic velocities in the upper-plate mantle are similar beneath the orogenic belt and in the hinterland. **B)** Divergence between upper plate and accretionary wedge triggers the exhumation of (U)HP rocks and the emplacement of serpentinized mantle-wedge rocks at shallow depth. Erosion on top of the (U)HP dome is minor at this stage, shortening is negligible. Because of widespread serpentinization of the mantle wedge during subduction, seismic velocities will be lower in the mantle-wedge rocks beneath the (U)HP dome, and higher in the adjoining dry mantle rocks of the upper plate.